Enhancing Electrochemical Performance of Zinc-Air Batteries Using Freeze Crosslinked Carboxymethylcellulose-Chitosan Hydrogels as Electrolytes

María Fernanda Bósquez-Cáceres,[1,]* **José Bejar,**[2] **Lorena Álvarez-Contreras,**[2] **and Juan P. Tafur**[1,z]

[1]*Grupo de Investigación Aplicada en Materiales y Procesos (GIAMP), School of Chemical Sciences & Engineering, Yachay Tech University, Urcuquí 100115, Ecuador*
[2]*Centro de Investigación en Materiales Avanzados S.C. (CIMAV), Miguel de Cervantes No. 120, Complejo Industrial Chihuahua, Chihuahua 31136, Mexico*

Zinc-air batteries (ZABs) are devices of great interest as a replacement option for subsequent technologies to lithium-ion batteries. Still, the need for suitable electrolyte materials limits their application in commercial devices. In this study, a green hydrogel composed of chitosan and carboxymethylcellulose was synthesized with the use of citric acid as a chemical crosslinker, physical freezing-thawing, and freezing-drying strategies. Physicochemical, thermal, and electrochemical characterizations were performed to study the effects of the proposed synthesis' on the performance of the hydrogels for the desired application. The obtained hydrogels showed a porous morphology that was doped with a 12 M KOH solution. Adequate complexation of K^+ cations and the polymer chains was observed. The resulting membranes showed an enhanced ionic conductivity of 0.39 S cm^{-1}, attributed to the pores and channels generated by the crosslinking strategies, contributing to the pathways for ions to move easily. In addition, the temperature dependence of the conduction mechanism was confirmed in the temperature range of 0 °C to 70 °C. The electrolytes were employed in ZABs prototypes, achieving a maximum power density of 117 mW cm^{-2} and a specific capacitance of 1899 mAh g^{-1}. The presented results show the promising properties of these hydrogels as electrolytes for green storage devices.

Zinc-air batteries (ZABs) have attracted considerable interest as an energy storage device for a wide range of applications. These batteries employ zinc as the negative metal electrode and an air-breathing positive electrode, and the advantages of this metal include inherent safety, low cost, and availability.[1] To develop a suitable ZAB prototype that can be scalable to commercial use, it is essential to have an appropriate electrolyte to connect both electrodes. Polymer electrolytes (PEs) are an important and promising technology for energy storage devices applications. These materials are a type of solid-state or gel-based matrix employed as the electrolyte component of a battery. PEs are known to be less volatile and non-flammable, leading to safer cells than conventional liquid electrolytes, avoiding some undesired reactions that provoke internal shorting, electrolyte leakage, and production of harmful gases.[2]

Several polymer matrixes designed to retain plasticizers or liquid electrolytes have been researched to improve their performance in ZABs.[3] Electrolytes made of biopolymers have shown comparable ion conduction and electrochemical properties than the traditional fossil-based polymer matrixes.[4–6] Their abundance, low cost, and easier processing ability make biopolymer electrolytes expected to be the next generation of green energy technologies. Among the available biopolymers, carboxymethylcellulose (CMC), and chitosan (CS) have been reported to form intermolecular complexes through strong electrostatic and hydrogen bonding interactions.[7,8] CMC-CS hydrogels can be synthesized through chemical and physical crosslinking. Chemical crosslinking has been the focus of our previous work employing citric acid (CA) as a chemical crosslinker,[9] which allowed us to obtain better structural integrity, higher thermal stability, and enhanced electrochemical properties. A maximum ionic conductivity value of 0.19 S cm^{-1} at 30 °C was achieved, along with a power density of 85 mW cm^{-2}.

Physically crosslinked hydrogels are synthesized by different strategies that lead to ionic interactions between the polymers, crystallization (freezing strategies), the formation of hydrophobic polysaccharide stereocomplexes, protein interaction, and hydrogen bonding.[10] Physical hydrogels can be obtained by repeated freeze-thaw (F-T) cycles from a concentrated aqueous solution containing polymers capable of forming physical crosslinks through weak interactions.[11] During freezing, the formed ice crystals organize the polymer chains around themselves. Then, during the thawing of the cycle, the ice crystals melt, giving rise to a microporous structure.[12] The stability of hydrogels obtained by this method increases with the number of F-T cycles.[13] From the works reported to date, in which chitosan hydrogels are synthesized by this technique, a decrease in pore size and an increase in elastic modulus and tensile strength are evidenced.[14–16]

On the other hand, freeze-drying through lyophilization is another inexpensive physical crosslinking method in which the sublimation process at low temperatures and under vacuum conditions produces homogeneous porous polymeric membranes with reduced shrinkage and high mechanical strength.[17] Zhong et al.[18] designed a porous methyl cellulose-based gel polymer electrolyte fabricated through freeze-drying that exhibited high ionic conductivity, low interface impedance, and low activation energy for Li$^+$ migration due to the presence of micropores in the matrix, capable of retaining large volumes of liquid electrolyte.

In the present study, membranes were synthesized from CS, CMC, and CA by freezing-thawing and posterior freeze-drying procedures. The synthesized membranes were doped with a 12 M KOH electrolyte solution. The physicochemical, thermal, and electrochemical properties of the hydrogels were determined to analyze the effect of the chemical and physical crosslinking strategies employed and to evaluate the applicability of the material as an electrolyte in ZABs. Then, a cell prototype was constructed with each membrane to perform primary battery tests to investigate the bulk resistance, the power and current densities, and the specific capacity of the cell prototypes with the designed materials.

*Electrochemical Society Student Member.
zE-mail: jtafur@yachaytech.edu.ec

Experimental

Chemicals and materials.—Carboxymethyl cellulose sodium salt (high molecular weight, high viscosity grade, sodium glycolate max. 0.4%), and anhydrous citric acid (CA) (purity 99.5%) were purchased from Loba Chemie. 90.6% deacetylated[19] chitosan food grade (low molecular weight, purity 100%, BioFitnest). Anhydrous glacial acetic acid for analysis (purity 100%) and potassium hydroxide pellets (purity ⩾ 85.00%) were purchased from Sigma Aldrich. All chemicals were used directly without further purification, and distilled water was used to prepare all the aqueous solutions. For electrochemical testing, Zn discs (99.99%) and Pt plates (99.97%) were acquired from Goodfellow. For the battery prototype, the anode was built of a piece of polished high-purity Zn foil of 0.2 mm thick, 10 × 15 mm width and length (purity 99.9%, Yunexpress Inc., Shenzhen). SIGRACET® 39 B slides of 0.4 mm thick, 10 × 15 mm width and length, impregnated with a catalyst mass loading of 1 mg cm^{-2} commercial catalytic ink and Pt/C (20% wt%) were designed as the cathode.

Preparation of the Frozen-Thawed CMC-CS-CA hydrogels.—Hydrogels were prepared by solution polymerization/crosslinking methods, following a procedure similar to the one previously reported by our research group,[9] and modified in this new work. We added 5 freeze-thawing cycles along with a freeze-drying step. Briefly, homogenous solutions of 2 wt% of CMC, 4 wt% of CA and 2 wt% of CS (in 1 wt% of acetic acid) were prepared separately. First, 90 ml CMC solution was mixed with 30 ml CS solution to form CMC-CSL solution. Then, varying amounts of the CA solution were added to form hydrogels named CA30L, CA40L, and CA50L (Table SI). The solutions were homogenized with an immersion blender for 3 min. Subsequently, the solutions were sonicated at 40 kHz at 60 °C for 1 h. The mixtures were then dried in an oven at 80 °C for 1 h. Excess liquid was removed starting the freezing-thawing cycle process. The solutions were frozen at −80 °C for 16 h, followed by thawing (room temperature for 8 h) for up to 5 repeated cycles. Finally, all hydrogels were freeze-dried for 48 h at −55 °C, 76 mmtorr in a lyophilizer (Gperon), and stored in a desiccator for characterization. One set of membranes was immersed in a 12 M KOH solution for 48 h for testing. The synthetis procedure is shown in Figure 1. Hydrated membranes are labeled with "sw" next to the names of the hydrogel (Table SI).

Physicochemical characterization.—X-ray diffractograms were obtained using a computer-controlled Rigaku Mini-flex-600 with a D/tex Ultra 2 detector 26 (Rigaku, Tokyo, Japan) operated at 40 kV and 15 mA in a sealed tube with a Ni-filtered Cu Kα radiation source (λ = 0.15418 nm). The studied angular region was 2θ = 5°–80° with a step width of 0.01°. Match! Software (Crystal Impact, Bonn, Germany) was used to quantify the crystallinity degree (CD) of the hydrogels.[20] Fourier transform-infrared (FTIR) was used to analyze the chemical bands of the hydrogels. IR spectra were obtained using a Cary 630 spectrophotometer equipped with a 1-bounce diamond ATR accessory (Agilent Technologies Inc.). The spectra were registered with 64 scans in the range of 4000–400 cm^{-1}, with a resolution of 4 cm^{-1}. Surface and cross-sectional scanning electron microscopy (SEM) micrographs were acquired with a JEOL JSM-6010/LV microscope (JEOL Ltd). Elemental mapping was performed on the swelled and used membranes by energy-dispersive X-ray spectroscopy (EDX) using an EDX TEAM analysis system integrated into the SEM. Thermogravimetric analysis was performed by a TGA SDT Q600 (TA Instruments), with a nitrogen flow from ambient to 800 °C using a heating ramp of 10 °C·min^{-1}. KOH swelling retention tests were carried out by weighing the membranes before and after 48 h of being immersed in the 12 M KOH solution, and the swelling ratio (SR) calculations were performed using Eq. 1:

$$SR = ((W_T - W_0)/W_0) \times 100\% \qquad [1]$$

where W is weight or volume, and the subindexes T and 0 represent the swollen membrane and the initial membrane, respectively. The initial and final volume of the hydrogels was measured by obtaining the length, width, and height of the sample with the use of a micrometer and multiplying these measurements to calculate the volume of a box-shaped figure.

A biodegradation study in composted soil was conducted using commercial soil employed for cultivation, following a similar method as the one reported by Michelle et al.[21] Membranes of 1.0 cm^2 and ∼0.5 cm were interred in the soil at room temperature in triplicate. Soil was watered every 3 d. Samples weights were registered at different time intervals after vacuum drying for 24 h.

Electrochemical measurements.—Electrochemical assays were performed using a VIONIC instrument (Metrohm model). Cyclic voltammograms (CV) were obtained at a sweep rate of 50 mV s^{-1} in a symmetrical potential window from −1.5 to +1.5 V using a symmetrical two-electrode Zn/hydrogel/Zn cell with 0.5 cm^2 non-blocking Zn electrodes. Potential electrochemical impedance spectroscopies (EIS) of the swollen hydrogels were obtained in the frequency range from 100 kHz to 1 Hz using a Pt/hydrogel/Pt cell configuration with 1 cm^2 Pt blocking electrodes. Impedance was measured over a temperature range from 0 °C to 70 °C with an accuracy of ±1 °C using a Julabo Polyscience circulator (−40 °C, 15 L) to calculate the ionic conductivity with Eq. 2:

$$\sigma = l/(A \times R_b) \qquad [2]$$

where A is the Pt electrode area, l is the film thickness, and R_b is the bulk resistance, obtained from the intersection of the impedance curve with the x-axis. Four measurements were performed for each membrane and temperature. The activation energy (E_a) was determined with Arrhenius Eq. 3 fitted linearly by plotting the logarithmic relationship between ln(σ) and 1000/T:

$$\sigma = \sigma_0 \times (-E_a/(T \times K_b)) \qquad [3]$$

where T is the absolute temperature, σ_0 is a pre-exponential factor, and K_b is the Boltzmann's constant.[22]

Zn-air battery tests.—The battery prototype tests were performed in an AMETEK® VersaSTAT 3 potentiostat/galvanostat (Princeton Applied Research). The hydrogels were placed between the Zn-Pt/C electrodes using the previously reported configuration,[23] without the use of the reservoir. Firstly, EIS spectra were obtained at the open circuit potential in a frequency range of 100 kHz to 0.1 Hz. Then, ZAB experiments like polarization and power density curves were performed for each membrane. The discharge current density for the polarization curves was 20 mV s^{-1}, and the cut-off voltage was 0.2 V. Additionally, the battery was discharged using different current densities maintained for 300 s. Finally, specific capacity was determined by applying a constant current density of 3 mA cm^{-2}, the zinc mass loss from this test, and the previously reported equation.[24]

Results and Discussion

Structural characterization.—XRD and FTIR studies In the obtained diffractograms, the peak at 10.2°, reported to be assigned to the amine I "–N–CO–CH$_3$" of chitosan,[25] had almost disappeared from the XRD patterns. The most prominent peak appeared at 2θ = 21.3°, with a broader shape compared to that of the pure polymers (Fig. 2), which is an indication of amorphization. The shift in this peak indicated the pairing of the CMC and CS chains by ionic interaction between the carboxyl groups from CMC and the amine groups from CS. It was reported that 2θ = 20.01° was assigned to the amine II (−NH$_2$) and to crystallographic planes (020), (110) and (120).[26] The shift presented towards higher theta values indicates a decrease in interchain spacing, typical of enhanced crosslinking.[27]
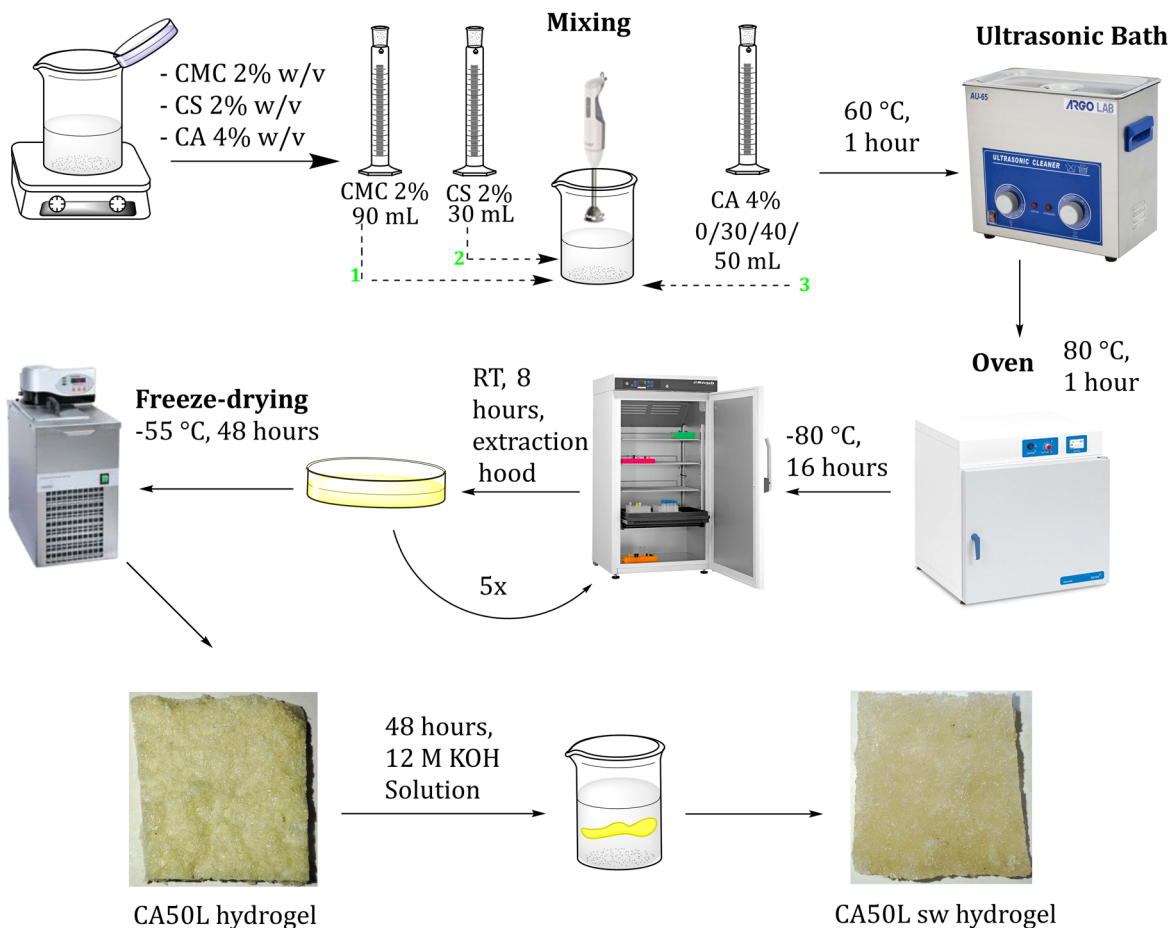
Figure 1. Scheme of the synthesis process of the CMC-CSL membranes as hydrogels for electrolytes.
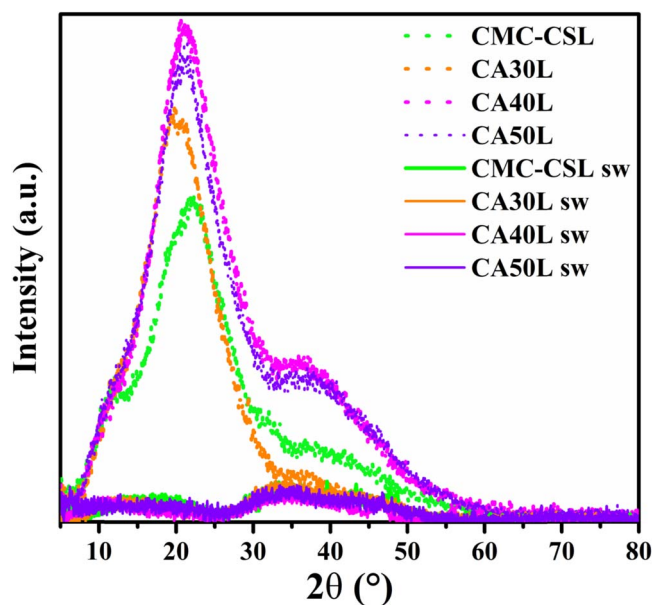
Figure 2. XRD patterns of the CMC-CSL and CMC-CSL sw hydrogels at different CA proportions.

The CA crosslinked membranes demonstrated an increase in the peak intensity for $2\theta = 21.3°$, and when compared to the CA-free hydrogel, an increase in the material's crystalline degree is evidenced, confirmed quantitatively with the CD obtained with Match! Software,[20] with values from 18.6% for the membrane without CA, up to a value of 24.2% for the CA50L membrane (Table I). This increase was especially evident in the peak $2\theta = 36.7°$ in the CA40L and CA50L membranes. The obtained XRD patterns are congruent with those published in the literature for similar polymeric matrices and pure polymers.[28,29] In terms of the hydrated hydrogels, the CD decreased due to the addition of KOH molecules to the matrix, since the K^+ cations form complexes with the polymer chains, breaking some of the hydrogen bonding in the system.[30]

Among the identified bands in the FTIR spectra, the CMC-CSL membrane depicted the characteristic bands for both polymers in the IR spectrum at 3200 and 3300 cm^{-1}, assigned to the –OH/NH stretching vibrations of CMC/CS, respectively (Fig. 3a).[28] The peaks observed at 2880 and 2857 cm^{-1} correspond to asymmetric and symmetric C–H stretching vibration of the N- acetyl group.[31] The band at 1021 cm^{-1} is related to the C–O–C vibration of the pyranose ring.[32] The most significant change in the spectrum of this hydrogel compared to pure polymers is that the amide group (1655 cm^{-1}) of CS and the carbonyl group (1596 cm^{-1}) of CMC interact to form a band at 1574 cm^{-1}, which suggests the complexation of CMC-CS by ionic interaction between the COO^- group of CMC and NH_3^+ group of CS.[33]

In the case of the CA crosslinked membranes, the ester bond formation reported for the reaction mechanism[9] was also confirmed for the proposed synthesis, with the band located at 1711 cm^{-1}, with the band observed at lower frequency compared to the casting dried membranes. The intensity of the band among the three samples is also an indicator of chemical cross-linking degree. The band corresponding to the C–O–C shifted to lower wavenumbers (1015 cm^{-1}), but with an increase in intensity, which is attributed to physical crosslinking caused by the F–T cycles.[34]

Table I. Crystallinity degree (CD) calculated from the XRD patterns.

Hydrogels	CD(%)
CMC-CSL	18.6
CA30L	19.6
CA40L	23.5
CA50L	24.2
CMC-CSL sw	9.6
CA30L sw	6.8
CA40L sw	6.4
CA50L sw	7.6

As for the hydrated membranes (Fig. 3b), the bands related to the O–H region showed changes, principally with an increase in the band at 3306 cm^{-1} due to the water insertion, confirmed also by the band at 1636 cm^{-1}, assigned to the O–H bending mode of water.[35] The carbonyl band shifted to 1596 cm^{-1}, due to the formation of complexes with K$^+$ originated from KOH insertion.[36] The band at 1021 cm^{-1} corresponding to the C–O–C ether pyranose ring presented a higher intensity compared to the homologous casting-dried counterparts,[9] which suggests that the physical crosslinking originated from the F–T processes preserves the polymeric chains in the system. Besides these differences in intensity of ester and ether bands, all the other bands between cast-dried and F–T dried membranes showed no differences, as an indicator of how this drying method does not affect other interactions that occur between both polymers.

SEM micrographs and EDX characterization.—Surface and cross-section micrographs of the CMC-CSL (Fig. 4a) presented an irregular morphology, with disordered pores and a smoother surface. Granules were also identified on the surface. The CA40L membranes (Fig. 4b, a highly porous and more distributed structure, was observed pointing towards efficient miscibility between the employed biopolymers and CA. Concerning its casting counterpart,[9] the morphology obtained in this work showed smaller and denser pores, attributed to the physical crosslinking of the hydrogels due to the repetitive F–T cycles.[34] These results suggest that the crosslinking methods used play a significant role in the pore size and shape of the membranes, as previously reported.[37] This morphology is related to

the more KOH solution absorption capability of the hydrogels, with the expanding of the pores in the matrix. The micrograph of the CA40L sw membrane (Fig. 4bIII) exhibited granules all over the matrix, due to the absorbed ionic salt solution. These granules evidenced the KOH dispersion throughout the membrane, and the complexation of the electrolyte components. In the case of the CMC-CSL sw hydrogel (Fig. 4aIII) the system showed some granules present, but a more tubular morphology was obtained.

After the discharge test, EDX mapping was performed on the hydrogels (Fig. 5), where the material composition expressed as weight percentage was obtained (Table II). For both membranes, some Zn deposition was evidenced, with higher metal residue in the case of the CMC-CSL sw membrane, and the appearance of dendrites (Fig. S1), that are originated by heterogeneous nucleation and growth of the electrodeposited Zn during the discharge process. These dendrites could cause perforations in the system, leading to safety issues.[18] Better uniform dispersion of potassium was observed in the chemically crosslinked membrane.

Swelling behavior, volume changes and biodegradability.—To know the KOH absorption in hydrogels, the swelling ratio and volume changes of the hydrated membranes were obtained with Eq. 1. The largest change was presented for the CA-free hydrogel (1342 ± 105 wt%, 63.61 ± 0.07 vol%) (Table III). As the hydrogel was prepared with more CA, a decrease in the SR was obtained. This is in agreement with what is expected when a higher crosslinking density is achieved,[38] with the same trend for the cast-dried membranes. Nevertheless, the physically crosslinked hydrogels absorbed at least 6 times its weight (CA50L sw membrane) with a non-significant volume change (657 ± 42 wt%, 16.69 ± 1.30 vol%). The volume change is a critical evaluation parameter since it affects the design of the final battery prototype.

To study the changes in the liquid content of the hydrogels, the weight percentage was recorded over time at room temperature. Figure 6a displays these changes over 56 d. A period of weight gain attributed to the hygroscopic nature of chitosan and CMC was evidenced due to the absorption of moisture from the environment.[39,40] The hydrogels underwent a dehydration process after 25 d, reaching a maximum weight percentage of 28.6% for the CA50L sw hydrogel. Moreover, the CA50L sw electrolyte was folded (Fig. 6b) and released, preserving its initial shape without breakage, as a demonstration of the flexible nature of the membranes. The hydrogels biodegradability was analyzed by burying the membranes in soil for 39 d (Figs. 6c–6e). During the study time, the
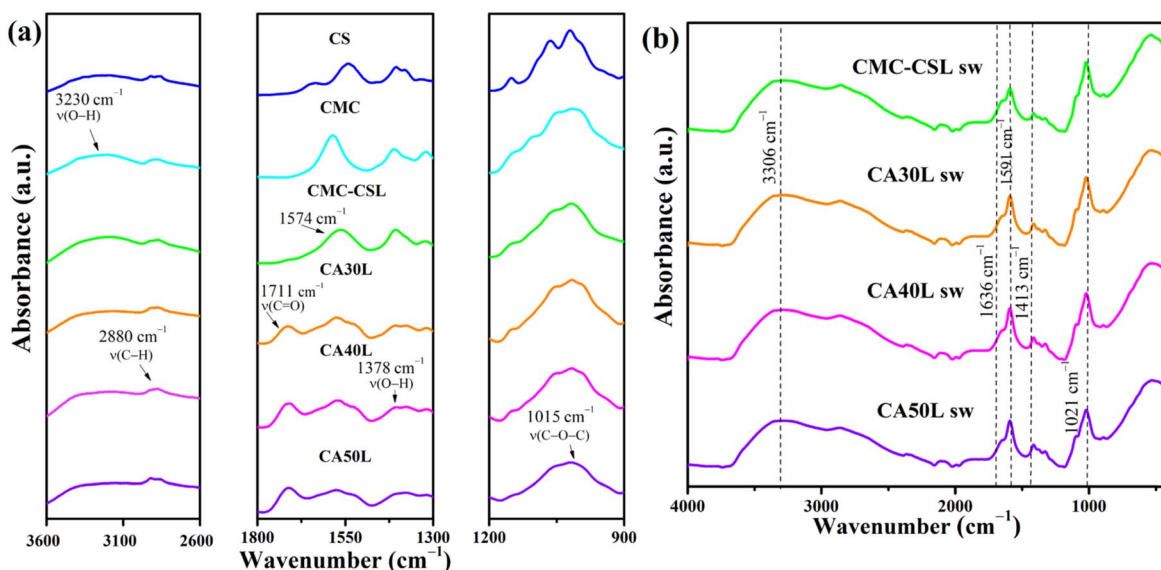
Figure 3. ATR-FTIR spectra of (a) CMC–CSL, and (b) CMC–CSL sw hydrogels at different CA proportions.
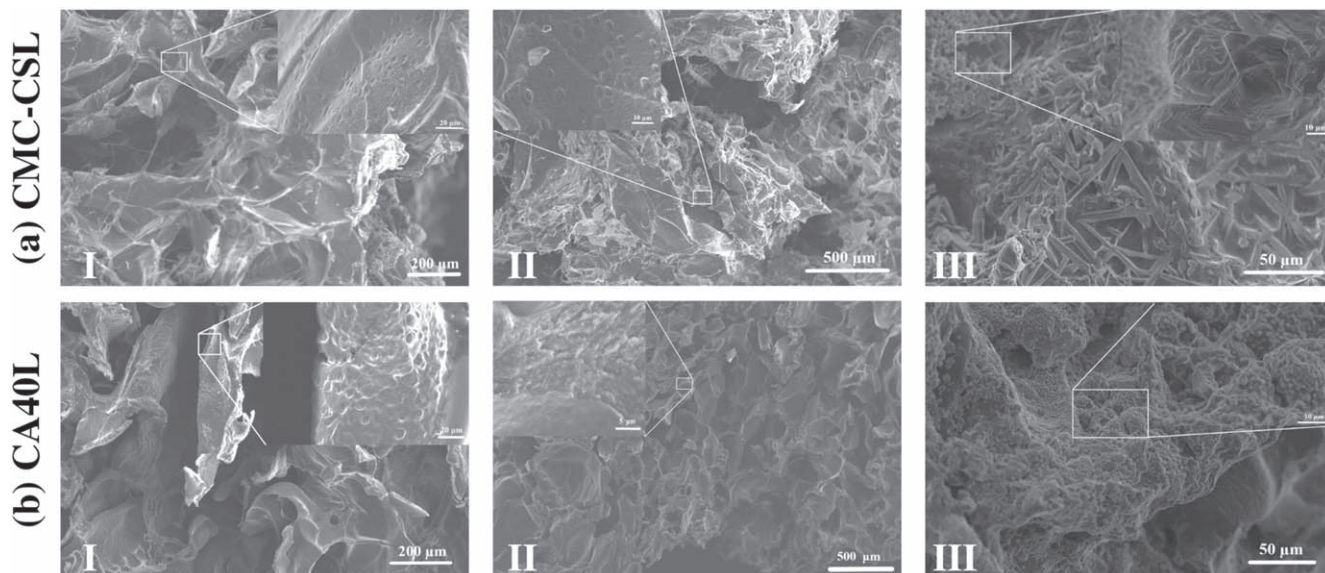
Figure 4. SEM micrographs of the dried (a) CMC-CSL and (b) CA40L hydrogel. Micrograph of the (I) surface, (II) cross section and (III) swollen in 12 M KOH.
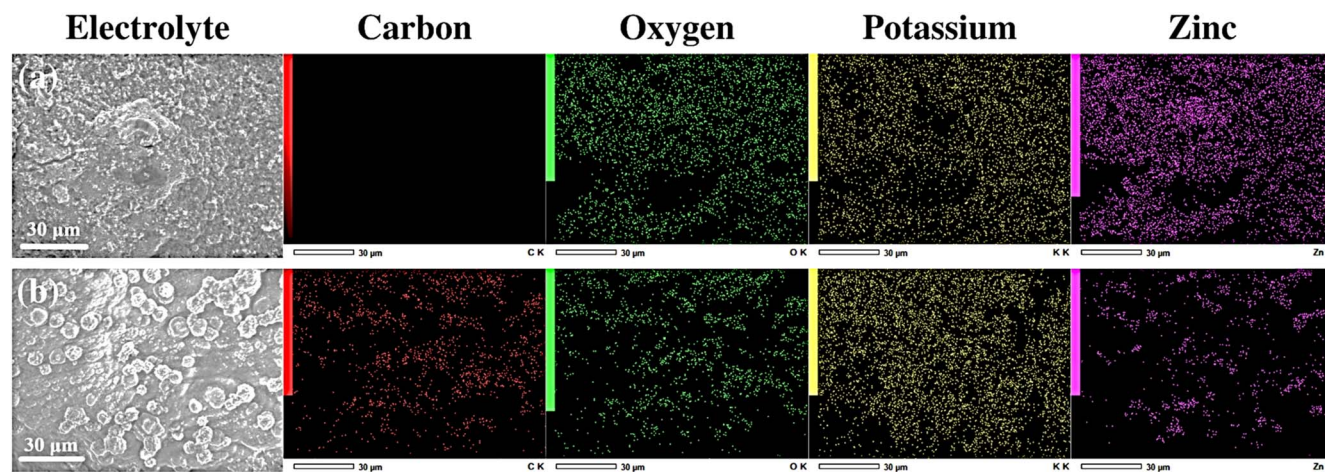
Figure 5. SEM images and EDX maps of (a) CMC-CSL sw and (b) CA40L sw in the cathode-facing side after discharging the Zn-air battery.

Table II. Material composition expressed as percentage by weight of the CMC-CSL sw and CA40L sw hydrogels in the cathode-facing side after discharging the Zinc-air battery.

Membrane	Material composition (Weight %)			
	Carbon	Oxygen	Potassium	Zinc
CMC-CSL sw	25.81	36.93	22.79	14.47
CA40L sw	26.35	32.52	38.08	3.06

Table III. Swelling behavior in mass percentage and volume change percentage of the synthesized membranes.

Electrolyte	Swelling Ratio (%)	Volume Change (%)
CMC-CSL sw	1342 ± 105	63.61 ± 0.07
CA30L sw	797 ± 38	18.77 ± 5.17
CA40L sw	743 ± 13	16.90 ± 4.56
CA50L sw	657 ± 42	16.69 ± 1.30

hydrogel started to degrade and became more malleable, and some mildew arose. By the weight retention measurements as a function of buried time (Fig. S2), the CA50L hydrogel lost 54.50% of its initial weight during the first 30 d of testing. A final remanent of 22.73% of weight was registered on day 39, where dirt got stuck on the membrane, making it difficult to assure an appropriate measurement after that. Moreover, the hydrogel's flammability was proved (Figs. 6e–6g), which demonstrates that when exposed to fire the membrane only shrugged, without explosions. This behavior is attributed to the non-flammable components employed for the hydrogel's fabrication.[41] The results indicate that these electrolytes are an option for developing green ZABs.

Thermal studies.—For the dry hydrogels, three degradation stages were identified (Fig. 7a). The first region, from 40 °C to 240 °C, corresponds to the process of loss of internal water. The weight of the hydrogel matrices only decreased by up to 15.1% between 30 °C and 200 °C. The second loss, up to 360 °C, is attributed to the degradation of the polymeric matrix and char formation. The considerable weight loss between 240 °C to 400 °C was related to the partial degradation of CS, decarboxylation of CMC, and decomposition of CA.[42] The last region represents the complete decomposition of the organic components of the
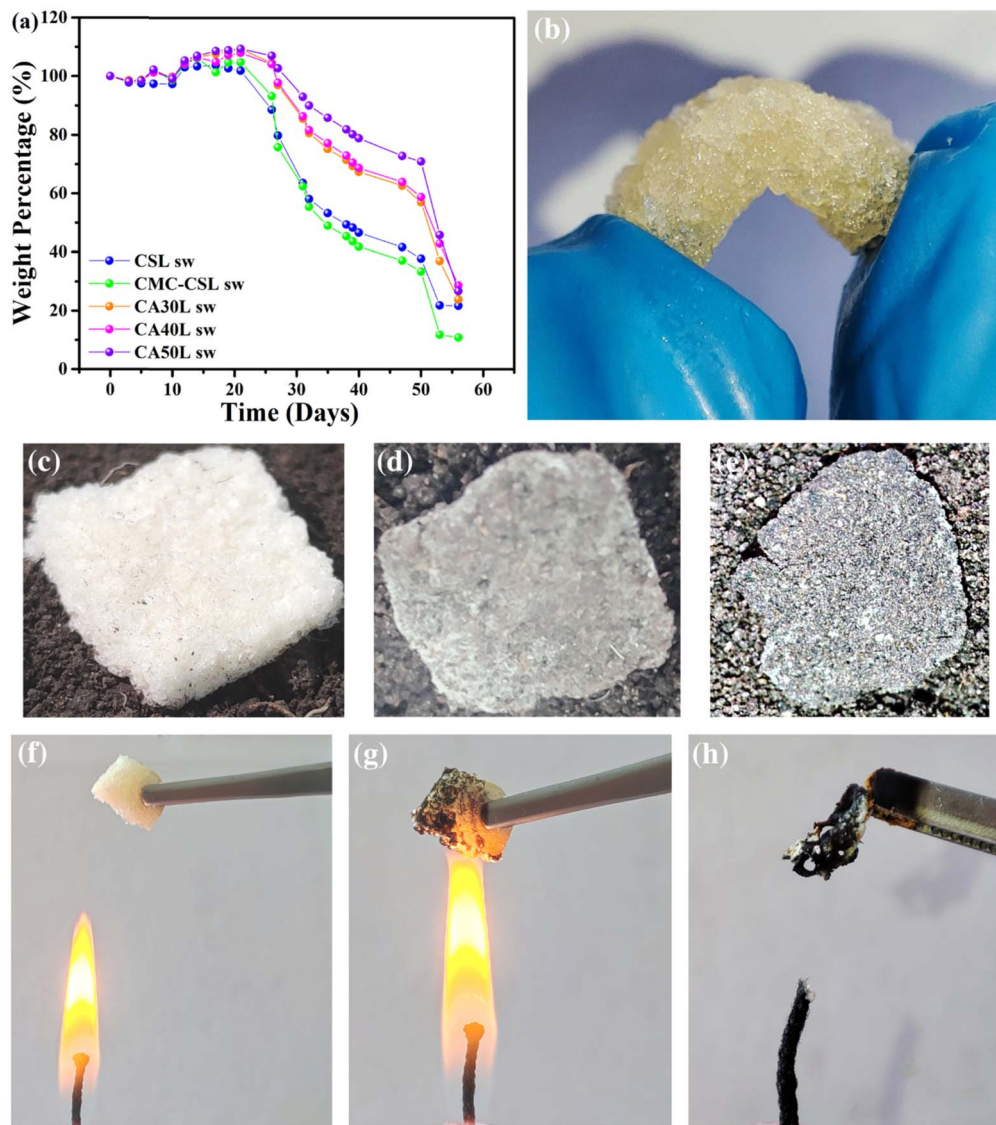
Figure 6. (a) Relation between the swollen membranes' changes with the storage time at ambient temperature. (b) Photograph of the CA50L sw hydrogel being bent to show its flexibility. Photographs of the CA50L electrolyte (c) fresh, buried in soil for (d) 30 d and (e) 39 d. (f) Photograph of the CA50L sw electrolyte prior to burning, (g) the CA50L sw electrolyte exposed to the flame, and (h) the hydrogel remanent after burning.
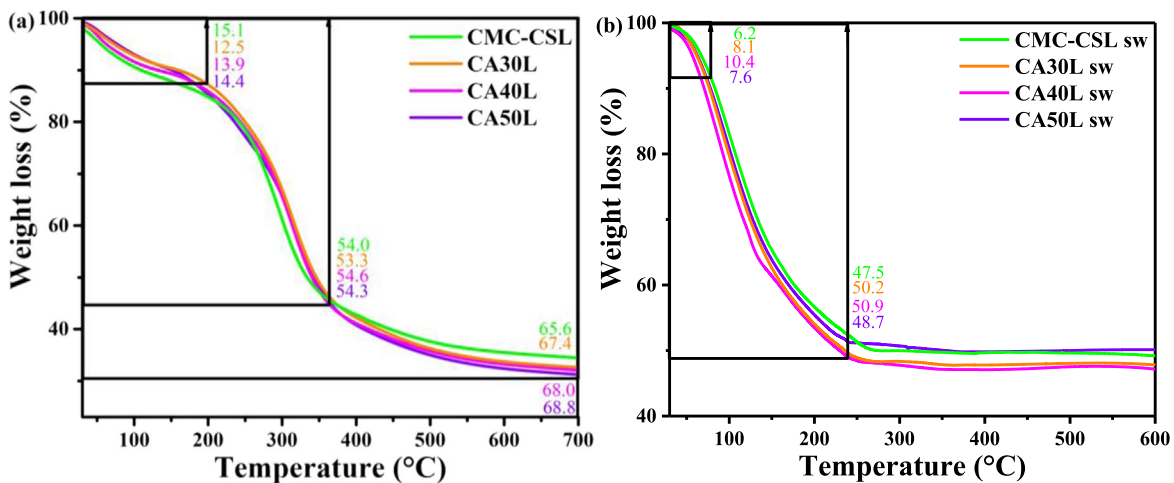
Figure 7. Thermogravimetric analysis curves of the (a) CMC-CSL and (b) CMC-CSL sw hydrogels.

hydrogels, with a stable weight from ∼550 °C onwards, with residues ranging from 34.4% for the CMC-CSL membrane to 31.6% for the CA50L hydrogel. The weight of the CA containing-membranes only decreased by less than ∼9% at 100 °C, which suggests the thermal stability of the matrices over the range of temperature applicability.

For the hydrated hydrogels, the first stage is related to the loss of water incorporated by the absorption of the KOH solution (Fig. 7b). From the DTGA curves (Fig. S3), it was evidenced that the minimum peak shifted to 101.1 °C for the most crosslinked membrane CA50L sw, increasing the thermal stability and water retention of the crosslinked biopolymeric membrane.[43] Nevertheless, this shift is smaller than the one previously obtained for its casting-dried counterpart.[9] The second region was found at 231.7 °C, 233.3 °C, 235.9 °C, 236.4 °C and 256.6 °C for the CA40L sw, CMC-CSL sw, CA30L sw, and CA50L sw, respectively, which corresponds to the degradation of the polysaccharide structure of the membrane.[44]

In the casting-dried hydrogels, there was an extra region at ∼537 °C that is absent in the TGA results presented. This step is related to the modification of the chemical structure by the oxygen-containing KOH molecule, which apparently does not occur in the proposed membranes. The hydrated membranes presented a higher residue percentage when compared to the dried membranes and were stable from ∼250 °C to the final test temperature, with the lowest loss of 47.5% for the CA30L sw hydrogel.

The DSC results (Fig. S4a) showed the apparition of an endothermic peak that increases in the range of 206 °C to 220 °C with the increase in the CA content, attributable to the heat absorption by thermal degradation of the polymers. Above 250 °C, the last peak becomes exothermic for all hydrogels, and becomes sharper as the CA content increases. The CA50L membrane showed the most endothermic nature, pointing to an enhancement of thermal stability, as a result of strong intermolecular interactions.[45] Swollen hydrogels (Fig. S4b) showed an increase in the intensity of the endothermic curve at 110 °C, indicating the formation of stronger internal bonds, implying that more heat is required to evaporate the absorbed water molecules. An exothermic peak was displayed at 250 °C, which could be associated with the decomposition of CS and of the amine unit.[29]

Electrochemical characterization.—Ion-conducting polymer electrolytes are characterized by the dissolving of salts in polar polymer matrices, as KOH complexed the synthesized membranes. In this context, the formed cations are expected to be responsible for ionic conductivity. Several models have been discussed to explain the conductive mechanism of these systems: Williams-Landel-Ferry (WLF) equation, Arrhenius equation, Effective Medium Theory (EMT), and Vogel-Tammann-Fulcher (VTF) equation.[46] Among them, Arrhenius's theory was confirmed by analyzing the relationship between the temperature and the ionic conductivity for all the hydrated membranes (Fig. 8a). The resulting cation transport mechanism is associated with the ions jumping to the nearest vacant sites, as occurs in ionic crystals, which results in a thermally assisted ionic conductivity mechanism.[47] The electrolyte membranes maintained the Arrhenius behavior until 70 °C, as an upgrade in contrast to the casting-dried membranes that lost it at 60 °C.[9] From the linear-fit equation, the activation energy (E_a) was calculated (Table IV), and an average of 0.12 eV was obtained, required by the ion so that it gets to move from one site to another in the conduction process.[48]

The ionic conductivity results have been analyzed in comparison to the SR (Fig. 8b), and the obtained values confirmed that KOH plays an imperative role in the system as it acts as the ionic species donor, increasing the ionic conductivity of the system when more KOH is present in the matrix. The highest ionic conductivity for the CA crosslinked membranes was 0.39 S cm^{-1} for the CA40L sw hydrogel. The obtained ionic conductivity values at 30 °C double the values reported in our previous study for the casting-dried membranes (0.19 S cm^{-1}),[9] even much higher than related reported works in the field, (less than 10^{-3} S cm^{-1}).[49–51] The enhancement
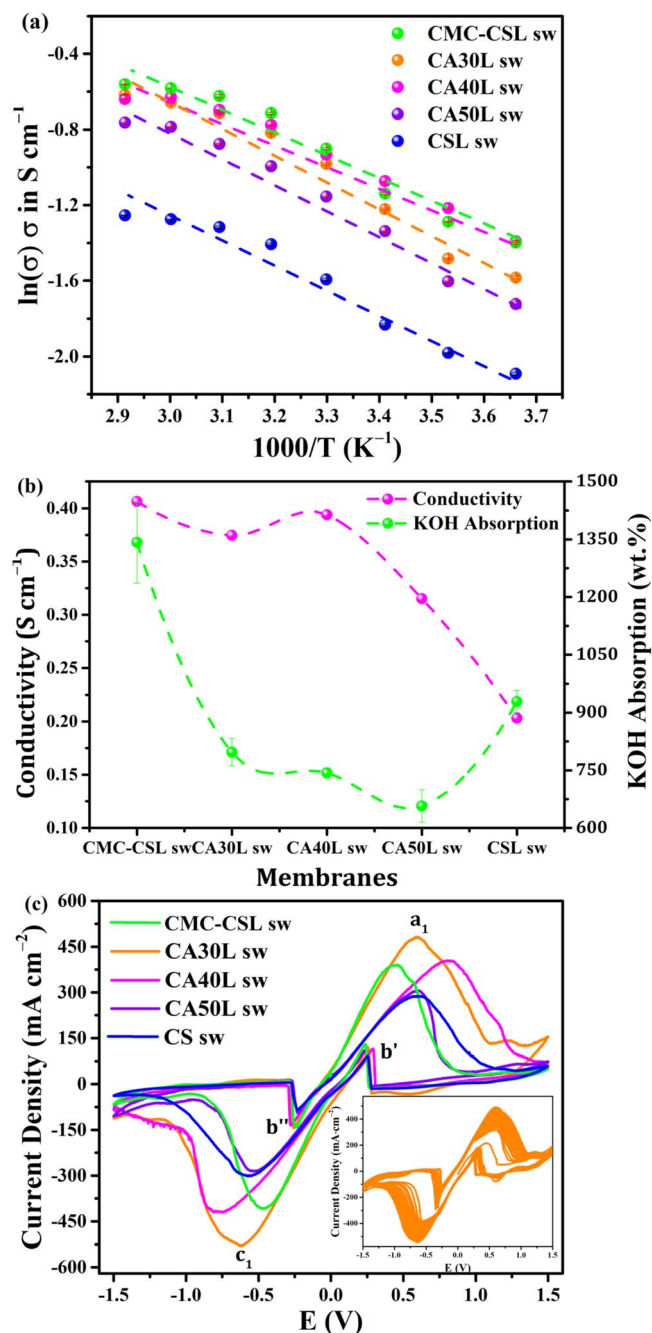
Figure 8. (a) Ionic conductivity of the CMC-CSL sw hydrogels at different temperatures. (b) Comparison between the ionic conductive values and swelling degree of the CMC-CSL sw hydrogels at different CA proportions. (c) Cyclic voltammograms of the swollen hydrogels at ambient temperature. Inset: 50 consecutive cycles of the CA30L sw hydrogels.

in the σ can also be explained in terms of the pores and channels generated by the physical crosslinking strategies since this obtained morphology provides paths for the ions to move more easily in the system.[52] In alkaline systems, as the one proposed, it is known that OH$^-$ is the specie that contributes to the ionic transport in the system. The pore sizes formed in the polymer matrix and the KOH concentration are the factors reported to be dependent on the anion transport.[53]

The cyclic voltammetry (CV) technique was used to analyze the electrochemical stability of the membranes, with a potential sweep in the range +1.5 to −1.5 volts. Figure 8c compares the voltammograms registered for the swollen hydrogels, where CA30L sw

Table IV. Electrochemical properties and battery performance for the hydrated hydrogels.

Electrolyte	E_a (eV)	σ(S cm^{-1})	ΔE_p (V)	Bulk resistance (Ω)	Specific capacitance (mAh g^{-1})	Power density (mW cm^{-2})
CMC-CSL sw	0.12	0.40	0.91	1.6	3.8	58
CA30L sw	0.13	0.37	1.21	1.5	1111	60
CA40L sw	0.10	0.39	1.59	2.0	1436	65
CA50L sw	0.13	0.32	1.14	1.4	1899	117
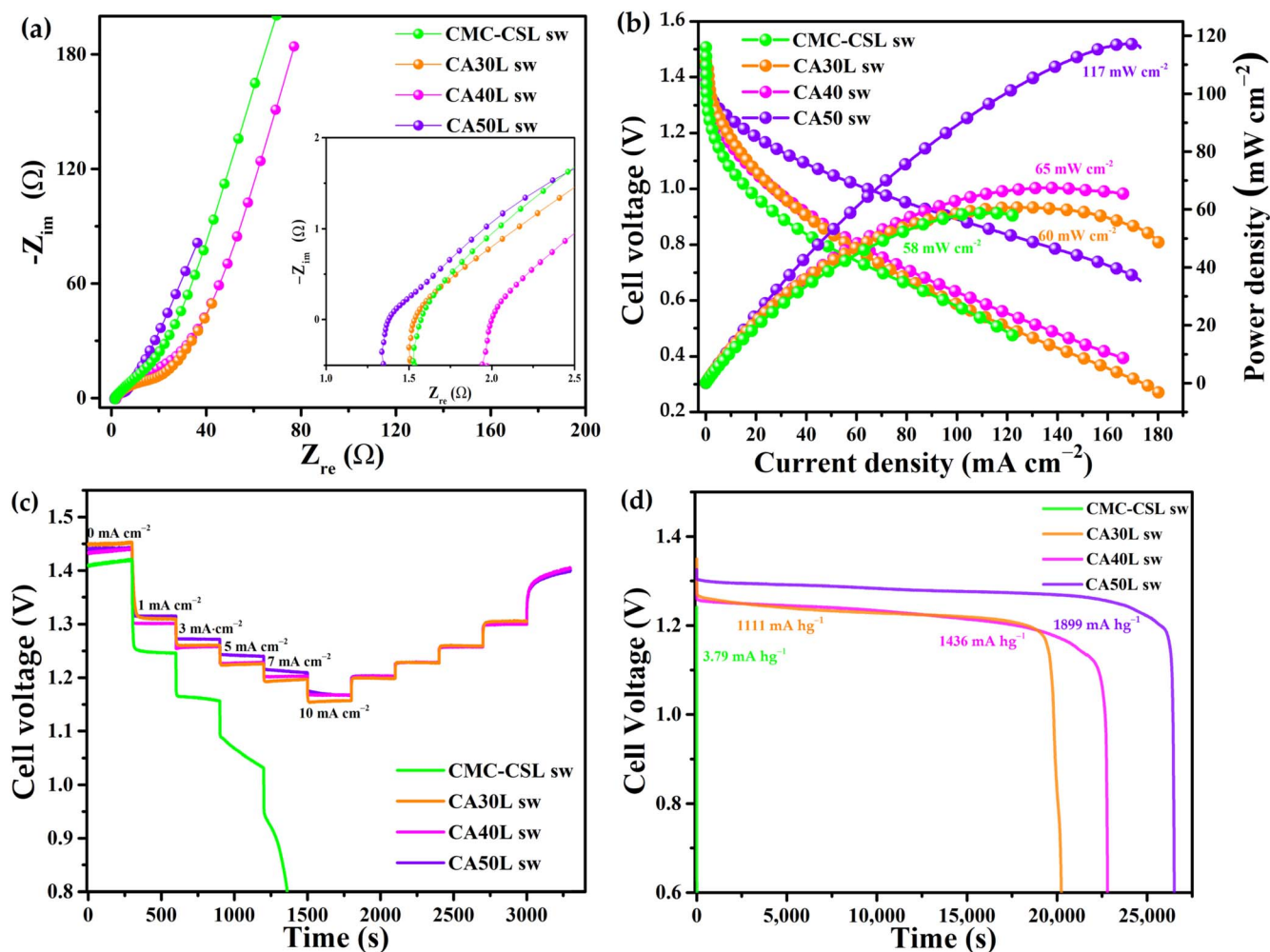
Figure 9. (a) Nyquist plot from PEIS studies (b) Polarization curves: discharge and power density profiles for the battery prototype and the synthesized hydrogels; (c) discharge tests at selected current densities; (C); (d) discharge curves at 3 mA cm^{-2}.

hydrogel presented the highest peak currents, with intensities higher than 450 mA cm^{-2} obtained. The reference electrode was connected in short-circuit to the counter electrode, with a large separation of the peak potentials due to this configuration. The anodic peak (a$_1$) is related to the zinc oxidation to Zn^{2+} cations in alkaline media, with the formation of Zn(OH)$_4^{2-}$, while the cathodic peak corresponded to the reduction process of this specie to solid Zn.[54,55] The b' inverse peak in the cathodic branch has been previously reported to appear in the cathodic sweep due to the Zn oxidation after the dissolution of some of the passive film formed on the Zn's electrode surface, with the equivalent process in the anodic sweep for the peak b'.[36] The potential difference (ΔE_p) was calculated to be in the range of 0.91 V to 1.59 V for the CMC-CSL sw and CA40L sw hydrogels, respectively (Table IV). From the 50 consecutive cycles (inset Fig. 8c), stability was evidenced by the peaks' shape with a quasi-reversible behavior. This tendency confirmed that the hydrogels are capable of Zn dissolution into the membranes, an essential step for

the ions' mobility in battery applications, corroborating the applicability of the synthesized hydrogels in energy devices.

Battery prototype testing.—For practical applications, the swollen hydrogels were tested as electrolyte in a ZAB prototype. Figure 9a exhibits the Nyquist plots, obtaining bulk resistances (Rb) values in the range of 1.4 Ω to 2.0 Ω (inset), which suggests a good electrical contact between electrodes across the synthesized membranes. Concerning the polarization curves (Fig. 9b, it is possible to distinguish the superior performance displayed by CA50L sw membrane, since it reached a current and maximum power densities o 172 mA cm^{-2} and 117 mW cm^{-2}, respectively. This superior performance obtained for the CA50L sw hydrogel could be explained by the higher chemical crosslinking degree achieved, and subsequent more density of functional groups in the structure of CA50L sw. The latter favors the intermolecular interactions with the liquid electrolyte, through the establishment of hydrogen bonds. These interactions lead to a greater stability of the

KOH solution in the polymer matrix, as discussed in the structural characterization section. Hence, this phenomenon is directly related to the higher ionic mass transport during the test process. Regarding the discharge at different demanded current densities (Fig. 9c), the CA50L sw electrolyte required the lowest overpotentials to deliver the fixed current, in addition to possessing an excellent recovery capability, because no significative changes were observed during the inverse process. Comparatively, the prototype with the CMC-CSL sw was only capable of supplying values of less than 7 mA cm^{-2}. Finally, the specific capacity test results are displayed in Fig. 9d, where the best result was obtained for the CA50L sw hydrogel with a capacitance of 1899 mAh g^{-1}. This value exceeded that reported for similar polymeric electrolyte systems. Poosapati et al.[56] obtained a maximum of 221.6 mAh g^{-1} for a gel-based polymer electrolyte composed of CS, polyvinyl alcohol (PVA) and KOH. The battery fabricated with the CMC-CSL sw hydrogel was not able to maintain performance during the discharge process. This collapse is attributed to the rapid formation of dendrites in this electrolyte (Fig. S1). It is suggested that these Zn dendrites were responsible for the early loss of the electrical connection with the Zn foil, leading to the early and severe loss of capacity of the prototype battery fabricated with the CMC-CSL sw membrane. In contrast, the CA-crosslinked membranes showed larger operation times, indicating their potential applicability in ZAB devices.

Conclusions

The design of a chemically and physically crosslinked CMC-CS hydrogel electrolyte doped with a 12 M KOH solution demonstrates its applicability of use in ZABs. The reticulation process was confirmed by ATR-FTIR, while the obtained XRD patterns pointed to the crystallinity changes that show the complexes formation between the K$^+$ cations and the polymer chains. SEM micrographs showed the porous morphology of the hydrogels and the appropriate complexation of the matrix with the doping salt. The hydrogel was fabricated with the proper combination of chemical and physical crosslinking techniques, resulting in a matrix with an enhanced ionic conductivity of 0.39 S cm^{-1}. The physical crosslinking achieved by the proposed freezing strategies is also enhancing the performance during the discharge process, attributed to the pores and channels generated, that contribute to the paths for the ions to be transported more easily. Arrhenius conduction mechanism was demonstrated from 0 °C to 70 °C. The high ionic transfer was confirmed by the CV studies, where the highest intensity peak of 480 mA cm^{-2} was obtained. A maximum power density of 117 mW cm^{-2} was achieved with the ZAB prototype assembled, besides a specific capacitance of 1899 mA hg^{-1}. These results demonstrate the potential of biopolymer hydrogels as electrolytes for green storage devices.

Acknowledgments

ORCID

Juan P. Tafur https://orcid.org/0000-0002-8944-2723

References

1. E. Davari and D. G. Ivey, *Sustain. Energy Fuels*, **2**, 39 (2017).
2. R. C. Agrawal and G. P. Pandey, *J. Phys. D: Appl. Phys.*, **41**, 223001 (2008).
3. F. Mo et al., *Batteries*, **8**, 59 (2022).
4. M. F. Bósquez-Cáceres, S. Hidalgo-Bonilla, V. M. Córdova, R. M. Michell, and J. P. Tafur, *Polymers (Basel).*, **13**, 4284 (2021).
5. S. Lorca, F. Santos, and A. J. Fernández Romero, *Polymers (Basel).*, **12**, 1 (2020).
6. M. Rayung et al., *Materials (Basel).*, **13**, 838 (2020).
7. N. Y. Bakar and M. I. N. Isa, *Res. J. Recent Sci.*, **3**, 74 (2014).
8. M. S. A. Rani, N. S. Mohamed, and M. I. N. Isa, *Int. J. Polym. Anal. Charact.*, **20**, 491 (2015).
9. M. F. Bósquez-Cáceres et al., *Batteries*, **8**, 265 (2022).
10. M. F. Akhtar, M. Hanif, and N. M. Ranjha, *Saudi Pharm. J.*, **24**, 554 (2016).
11. E. S. Dragan and M. V. Dinu, *React. Funct. Polym.*, **146**, 104372 (2020).
12. H. Zhang, F. Zhang, and J. Wu, *React. Funct. Polym.*, **73**, 923 (2013).
13. Y. Guan, J. Bian, F. Peng, X. M. Zhang, and R. C. Sun, *Carbohydr. Polym.*, **101**, 272 (2014).
14. M. T. Khorasani, A. Joorabloo, H. Adeli, Z. Mansoori-Moghadam, and A. Moghaddam, *Carbohydr. Polym.*, **207**, 542 (2018).
15. S. Noori, M. Kokabi, and Z. M. Hassan, *J. Appl. Polym. Sci.*, **135**, 46311 (2018).
16. M. T. Khorasani, A. Joorabloo, A. Moghaddam, H. Shamsi, and Z. MansooriMoghadam, *Int. J. Biol. Macromol.*, **114**, 1203 (2018).
17. L. Hu, R. He, Z. Lu, K. Zhang, and X. Bai, *RSC Adv.*, **9**, 9931 (2019).
18. G. Zhong et al., *Appl. Mater. Today*, **30**, 101705 (2023).
19. L. A. Calderón Salas, L. De Lima Eljuri, and M. Caetano Sousa, *Thesis*, Universidad de Investigación de Tecnología Experimental Yachay(Urcuqui) (2021).
20. H. Putz and K. Brandenburg, https://crystalimpact.de/match.
21. R. M. Michelle et al., *Macromolecules*, **42**, 6671 (2009).
22. R. B. Nuernberg, *Ionics (Kiel).*, **26**, 2405 (2020).
23. J. Béjar, L. Álvarez-Contreras, J. Ledesma-García, N. Arjona, and L. G. Arriaga, *J. Mater. Chem. A*, **8**, 8554 (2020).
24. J. Béjar et al., *Carbon N. Y.*, **204**, 411 (2023).
25. Y. Jampafuang, A. Tongta, and Y. Waiprib, *Polymers (Basel).*, **11**, 2010 (2019).
26. H. E. Salama, M. S. Abdel Aziz, and M. W. Sabaa, *Int. J. Biol. Macromol.*, **139**, 1162 (2019).
27. M. K. Jaiswal et al., *ACS Nano*, **10**, 246 (2016).
28. K. A. Uyanga, O. P. Okpozo, O. S. Onyekwere, and W. A. Daoud, *React. Funct. Polym.*, **154**, 104682 (2020).
29. K. A. Uyanga and W. A. Daoud, *Cellulose*, **28**, 5493 (2021).
30. A. A. Iles Velez et al., *Gels*, **7**, 256 (2021).
31. K. A. Uyanga and W. A. Daoud, *Int. J. Biol. Macromol.*, **181**, 1010 (2021).
32. Y. Zhang et al., *Chem. Eng. J.*, **353**, 225 (2018).
33. S. Benghanem, A. Chetouani, M. Elkolli, M. Bounekhel, and D. Benachour, *Biocybern. Biomed. Eng.*, **37**, 94 (2017).
34. C. Chang, A. Lue, and L. Zhang, *Macromol. Chem. Phys.*, **209**, 1266 (2008).
35. T. Seki et al., *J. Phys. Chem. Lett.*, **11**, 8459 (2020).
36. F. Santos, J. P. Tafur, J. Abad, and A. J. Fernández Romero, *J. Electroanal. Chem.*, **850**, 113380 (2019).
37. A. Autissier, C. Le Visage, C. Pouzet, F. Chaubet, and D. Letourneur, *Acta Biomater.*, **6**, 3640 (2010).
38. T. Fekete, J. Borsa, E. Takács, and L. Wojnárovits, *Radiat. Phys. Chem.*, **124**, 135 (2016).
39. E. Szymańska and K. Winnicka, *Mar. Drugs*, **13**, 1819 (2015).
40. M. D. Torres, R. Moreira, F. Chenlo, and M. J. Vázquez, *Carbohydr. Polym.*, **89**, 592 (2012).
41. M. Wu et al., *Matter*, **5**, 3402 (2022).
42. K. Dharmalingam and R. Anandalakshmi, *Int. J. Biol. Macromol.*, **134**, 815 (2019).
43. I. Farinha and F. Freitas, *Handb. Chitin Chitosan*, **3**, 43 (2020).
44. L. Song, F. Liu, C. Zhu, and A. Li, *Chem. Eng. J.*, **369**, 641 (2019).
45. K. Wang et al., *J. Food Sci. Technol.*, **56**, 5396 (2019).
46. G. Dlubek, D. Kilburn, and M. A. Alam, *Electrochim. Acta*, **49**, 5241 (2004).
47. S. B. Aziz, T. J. Woo, M. F. Z. Kadir, and H. M. Ahmed, *J. Sci. Adv. Mater. Devices*, **3**, 1 (2018).
48. M. Petrowsky and R. Frech, *J. Phys. Chem. B*, **114**, 8600 (2010).
49. T. Xu et al., *Energy Storage Mater.*, **48**, 244 (2022).
50. C.-L. Hung, M. Chen, M. I. H. Sohaimy, and M. I. N. Isa, *Polymers (Basel).*, **14**, 3019 (2022).
51. K. Jayalakshmi et al., *J. Phys. Chem. Solids*, **173**, 111119 (2023).
52. L. Cao et al., *Chem. Soc. Rev.*, **46**, 6725 (2017).
53. K. N. Grew and W. K. S. Chiu, *J. Electrochem. Soc.*, **157**, B327 (2010).
54. X. Liu et al., *Adv. Mater.*, **33**, 2006461 (2021).
55. J. Abad et al., *J. Power Sources*, **363**, 199 (2017).
56. A. Poosapati et al., *J. Appl. Polym. Sci.*, **138**, 50813 (2021).